Pulling force enabled by unlocking the optical phase

Andrei Kiselev [ORCID],[*] Siarhei Zavatski [ORCID], and Olivier J. F. Martin [ORCID][†]

Nanophotonics and Metrology Laboratory, Institute of Electrical and Microengineering,
École Polytechnique Fédérale de Lausanne, EPFL-STI-NAM Station 11, 1015 Lausanne, Switzerland

Karim Achouri [ORCID]

Laboratory for Advanced Electromagnetics and Photonics, Institute of Electrical and Microengineering,
École Polytechnique Fédérale de Lausanne, EPFL-STI-LEAP, 1015 Lausanne, Switzerland

We demonstrate the possibility of achieving an optical pulling force without complex beam-shaping techniques. By using optical pulses detuned from the resonant frequency of the structure, we create conditions in which the spectral maxima of the excited current and of the incident field do not match. Therefore, the phase shift between the two, which controls the optical force, becomes time dependent, thus enabling unexpected optical effects. Particularly, it is shown that tuning the central frequency of the pulse produces a temporary pulling force directed towards the illumination source.

I. INTRODUCTION

Is it possible to induce on an object an electromagnetic pulling force directed toward the illumination source? Interestingly, the contemporary answer to this question differs from the one that could be given in the 17th century. Back then, only optical pushing forces were known, e.g., as the primary explanation for the comet tail deviation away from the Sun [1,2].

Much later, in the second part of the 20th century, a series of works performed by the Nobel Prize winner A. Ashkin demonstrated the possibility of stable particle trapping with light [3,4]. This ability to trap [5–7] stimulated further research aimed at testing the limits of control over the position of an object in terms of pushing [8], pulling [9], lateral control [10–12], or a full three-dimensional (3D) manipulation [13]. Clearly, from the momentum conservation point of view, light can transfer momentum to an object, leading to a pushing force collinear with the light propagation direction. An opposite effect may *a priori* appear impossible: A photon traveling along one direction in the same medium cannot gain momentum from a passive time-invariant system. Therefore, only a pushing effect seems possible.

However, there are multiple approaches to circumvent this limitation and obtain optical pulling on an object [9]. The majority of them are related to the increment of the projection of momentum of a photon along a certain direction by means of structured light, thus providing a recoil pulling force on the object [9,14–16]. Other methods involve the use of photophoretic forces [17], blackbody radiation [18], Casimir forces [19], chirality [20–22], active media [23], plasmonic surfaces [24], photonic crystals [25], gratings [26], metama-

terials and metasurfaces [27–30], and resonance frequency detuning [31–33], among many others, as summarized in a review article [9]. These pulling effects are always associated with an average force that does not change over time.

Quite recently, temporal studies of optical forces in nanophotonics revealed a plethora of effects that stem from the intrinsic nonlinear character of electromagnetic forces. Indeed, excitation with continuous wave illumination at frequency ω_0 effectively produces an optical force that oscillates at frequency $2\omega_0$ [34]; optical forces in the time domain have many similarities to second harmonic and sum-frequency generations [35–37]. For example, for illumination with two slightly detuned waves ω_0 and $\omega_0 + \Omega$, the optical force acquires a frequency difference component at frequency Ω, which can lead to mechanical oscillations of macroscale [38–40] and microscale [41–48] objects. An interesting feature of multifrequency illumination is the enhancement of the instantaneous optical force caused by the beatings between different frequency components [34]. This effect was observed in experiments with atoms and molecules for two-frequency [38,49–53], four-frequency [54], and multifrequency [55] illuminations. In the case of nanoparticles, pulsed illumination can also lead to an enhanced instantaneous optical force that helps release stuck nanoparticles [56,57] or, alternatively, helps fuse them [58,59]. It was shown, however, that the total momentum transferred to the particle depends only on the pulse power and not on beating effects [60].

Time-dependent studies of optical pulling forces also revealed several interesting effects; for example, even a single plane wave impinging on a film under normal incidence can lead to a pulling effect that is reached for a fraction of the pulse cycle [34]. This temporal pulling appears periodically at frequency $2\omega_0$ and is related to the oscillating (reactive) component of the Poynting vector [61]. Since such a pulling effect can be reached only for a fraction of the period, the time-average force remains positive, which is consistent with the

---

[*]Contact author: andrei.kiselev@epfl.ch
[†]Contact author: olivier.martin@epfl.ch

195432-1

momentum conservation law [61]. One can also specifically tailor temporally decaying fields such that the processes of momentum transfer to the object and its back-conversion into forward-propagating photons are separated in time, leading to a temporal pulling effect over a few optical cycles [62].

Here, we explore a different approach to produce a pulling force based on the idea of dynamic phase variation. We first highlight in Sec. II the relation between the optical force and the phase shift between the incident field and the response of the structure. Generally, this phase shift is locked by the geometry of the structure when continuous wave illumination is applied; in this case, the average optical force is always positive. To overcome this limitation, in Sec. III we show an approach to dynamically change this phase shift by illuminating a structure with a pulsed laser with a central frequency slightly shifted with respect to the object's resonance frequency. We demonstrate in Sec. IV that in specific cases the phase shift starts to gradually change with time, leading to the reversion of the optical force (optical pulling) for a few optical cycles. Finally, we show in Sec. V other cases where either fully positive or alternating positive and negative forces can be achieved with a pulse and provide a comprehensive explanation of these effects.

II. OPTICAL FORCES AND THE ROLE OF PHASE

Let us recall the fundamentals of optical force analysis and provide a simple formula for an optical force acting on a subwavelength object. In what follows, we highlight that the phase difference $\Delta\varphi(\mathbf{J}, \mathbf{H}_i)$ between the current $\mathbf{J}(t)$ induced within the structure and the incident magnetic field $\mathbf{H}_i(t)$ in the structure is responsible for the direction of the optical force. Indeed, from the definition of the Lorentz force [61],

$$\mathbf{F}(t) = \int_V \text{Re}[\rho(\mathbf{r}, t)] \text{Re}[\mathbf{E}(\mathbf{r}, t)] \\ + \text{Re}[\mathbf{J}(\mathbf{r}, t)] \times \mu_0 \text{Re}[\mathbf{H}(\mathbf{r}, t)] dV, \quad (1)$$

where $\rho(\mathbf{r}, t)$ is the charge density, $\mathbf{E}(\mathbf{r}, t)$ and $\mathbf{H}(\mathbf{r}, t)$ are the total electric and magnetic fields, $\mu_0 = 1.26 \times 10^{-6} \frac{H}{m}$ is the magnetic permeability of vacuum, and integration is performed over the volume V of the object. Also, we assume vacuum as the background throughout. Let us simplify Eq. (1) by taking into account that the object is subwavelength and that the incident wave is a plane wave propagating along the z axis. In general, the electric, $\mathbf{E}(\mathbf{r}, t)$, and magnetic, $\mathbf{H}(\mathbf{r}, t)$, fields in Eq. (1) can be represented as a sum of the incident (i) and scattered ones (s) as

$$\mathbf{E}(\mathbf{r}, t) = \mathbf{E}_i(\mathbf{r}, t) + \mathbf{E}_s(\mathbf{r}, t), \quad (2)$$

$$\mathbf{H}(\mathbf{r}, t) = \mathbf{H}_i(\mathbf{r}, t) + \mathbf{H}_s(\mathbf{r}, t). \quad (3)$$

The charges and current are related to the fields as

$$\rho(\mathbf{r}, t) = \varepsilon_0 \nabla \cdot \mathbf{E}(\mathbf{r}, t), \quad (4)$$

$$\mathbf{J}(\mathbf{r}, t) = \frac{1}{\mu_0} \nabla \times \mathbf{B}(\mathbf{r}, t) - \varepsilon_0 \frac{\partial \mathbf{E}(\mathbf{r}, t)}{\partial t}. \quad (5)$$

Here, $\varepsilon_0 = 8.85 \times 10^{-12} \frac{F}{m}$ is the permittivity of vacuum. By inserting Eqs. (2)–(5) into Eq. (1), we obtain the force as a result of interactions between the incident field and itself,

the incident-scattered fields, and the scattered-scattered fields. The supplement of Chen *et al.* [63] showed that the incident field does not produce an optical force on interacting with itself. Indeed, without a scattering response, there can be no force. Additionally, the scattered-scattered interaction is zero when we assume only an electric dipolar response: An isolated dipole radiates symmetrically and cannot produce an optical force on its own. If we assume that the object scatters only as an electric dipole (valid for subwavelength metallic nanoparticles), the force arises only due to the interaction between the incident and scattered fields; see Eq. (39) of the supplement of Ref. [63]. Let us focus on the force along the z axis, which can be either pushing or pulling. It can simply be verified that since the field propagates along the z axis, the first component in Eq. (1) is zero as there is no field along the z axis. Thus, the optical force along the z axis takes the form

$$\mathbf{F}_z(t) = \int_V \{\text{Re}[\mathbf{J}(\mathbf{r}, t)] \times \mu_0 \text{Re}[\mathbf{H}_i(\mathbf{r}, t)]\}_z dV. \quad (6)$$

For a subwavelength object, the fields and currents in Eq. (6) can be approximated by their values at the center of the structure, $\mathbf{H}_i(\mathbf{r}, t) \approx \mathbf{H}_i(\mathbf{r} = 0, t) = \mathbf{H}_i(t)$ and $\mathbf{J}(\mathbf{r}, t) \approx \mathbf{J}(\mathbf{r} = 0, t) = \mathbf{J}(t)$. Let us assume that the object is illuminated at a single frequency ω_0 with $e^{-i\omega_0 t}$ dependence. Let us then find the time average of Eq. (6) by using the following definition: $\langle C(t) \rangle = \frac{1}{T} \int_0^T C(t) dt$, where the averaging is performed over the period of the wave $T = 2\pi/\omega_0$. Using the fact that for two arbitrary complex numbers A and B the relation $\text{Re}(A) \text{Re}(B) = \frac{1}{2} \text{Re}(AB + AB^*)$ (where $*$ stands for the complex conjugate) holds, Eq. (6) can be similarly separated into two terms. The first one, $\text{Re}(AB)$ in Eq. (6), is proportional to $\text{Re}[\mathbf{J}(t) \times \mathbf{H}_i(t)] \sim \text{Re}(e^{-2i\omega_0 t})$. This term gives zero on averaging over a period T. The time-average term in Eq. (6) is then attributed to the $\text{Re}(AB^*)$ part and reads

$$\langle \mathbf{F}_z(t) \rangle_T = \frac{1}{2} \mu_0 \{\text{Re}[\mathbf{J}(t) \times \mathbf{H}_i^*(t)]\}_z V. \quad (7)$$

For what follows, it is important to emphasize that for light scattering, the response of an object, described here by the current $\mathbf{J}(t)$, is usually dephased with a factor $\Delta\varphi$ with respect to the excitation—here the incident magnetic field $\mathbf{H}_i(t)$ [64]. This phase shift depends on the scatterer and on the excitation conditions.

We consider a harmonic incident magnetic field $\mathbf{H}_i(t) = \mathbf{H}_{i,0} e^{-i\omega_0 t}$ and the current retarded by $\Delta\varphi(\mathbf{J}, \mathbf{H}_i)$, $\mathbf{J}(t) = \mathbf{J}_0 e^{-i\omega_0 t} e^{i\Delta\varphi(\mathbf{J}, \mathbf{H}_i)}$, where $\mathbf{H}_{i,0} \in \text{Re}$, $\mathbf{J}_0 \in \text{Re}$ and we have introduced the phase shift $\Delta\varphi(\mathbf{A}, \mathbf{B}) = \Delta\varphi(\mathbf{A}(t), \mathbf{B}(t)) = \arg[\mathbf{A}(t)/\mathbf{B}(t)]$. Here, arg is the argument of the complex value. The time-average optical force then reads

$$\langle \mathbf{F}_z(t) \rangle_T = \frac{1}{2} \mu_0 [\mathbf{J}_0 \times \mathbf{H}_{i,0}]_z \cos[\Delta\varphi(\mathbf{J}, \mathbf{H}_i)] V. \quad (8)$$

Therefore, the phase $\Delta\varphi(\mathbf{J}, \mathbf{H}_i)$ determines the direction of the time-average optical force. The total *instantaneous* force along the z axis has the following form:

$$\mathbf{F}_z(t) = \frac{1}{2} \mu_0 [\mathbf{J}_0 \times \mathbf{H}_{i,0}]_z \text{Re}(e^{-2i\omega_0 t + i\Delta\varphi(\mathbf{J}, \mathbf{H}_i)}) V. \quad (9)$$

Let us analyze the time-dependent and average terms in Eq. (9), taking as an example a silver nanoparticle with the radius $R = 10$ nm illuminated with an x-polarized plane wave. The scattering cross section (SCS) corresponding to this
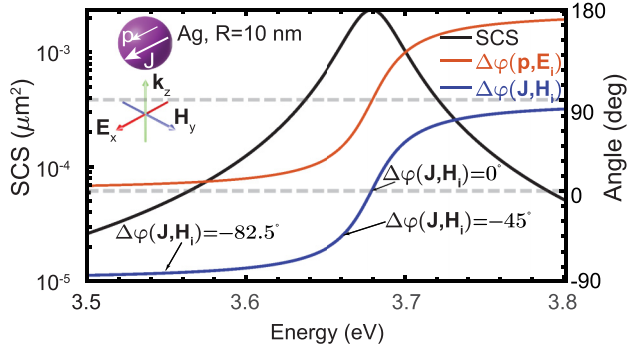
FIG. 1. Scattering cross section (SCS, black line) of an isolated Ag spherical nanoparticle with radius $R = 10$ nm. Relative phase difference $\Delta\varphi(\mathbf{p}, \mathbf{E}_i)$ (orange line) between the electric dipole excited in the nanoparticle and the incident electric field $\mathbf{E}_i$ as well as the relative phase difference $\Delta\varphi(\mathbf{J}, \mathbf{H}_i)$ (blue line) between the current $\mathbf{J}$ induced within the object and the incident magnetic field $\mathbf{H}_i$.

situation is shown by a solid black line in Fig. 1. For such a system, only a single electric dipole is excited [65]. This dipole can be described by a damped harmonic oscillator model [66], which classically predicts the phase shift between the electric dipole $\mathbf{p}$ and the incident electric field $\mathbf{E}_i$ within the limits $\Delta\varphi(\mathbf{p}, \mathbf{E}_i) \in [0, 180°]$ (see the orange curve in Fig. 1) [61,67]. Indeed, for a mass m_h on a spring with spring constant k_h and losses Γ_h that is excited by a harmonically oscillating force $F(t) = F_h e^{-i\omega_0 t}$, the equation of motion is

$$m_h \frac{d^2 x}{dt^2} + \Gamma_h \frac{dx}{dt} + k_h x = F_h e^{-i\omega_0 t}. \tag{10}$$

The solution for this equation is

$$x(\omega_0, t) = \frac{F_h/m}{(\omega_h^2 - \omega_0^2) - i\omega_0\Gamma_h/m} e^{-i\omega_0 t}, \tag{11}$$

with $\omega_h = \sqrt{k/m}$. For $\omega_0 \ll \omega_h$ and low losses, the phase shift between the coordinate x and the driving force is zero, and the first two terms of Eq. (10) do not contribute to the solution. The object therefore appears massless and lossless. For $\omega_0 \gg \omega_h$ the phase shift is $180°$ and is related only to the first term in Eq. (10). Hence, at high frequencies the presence of a mass introduces a phase shift. Finally, for $\omega_0 = \omega_h$, the losses introduce a phase shift of $90°$. This harmonic oscillator model is applicable for many systems, including plasmonics, and can be applied to the system at hand [64,68].

In plasmonics, the harmonic oscillator model usually describes the dipole excited in the system [68]; to obtain the current used in Eqs. (8) and (9), one has to recall that the electric dipole $\mathbf{p}$ and the current are related by $\mathbf{J} \sim d\mathbf{p}/dt = -i\omega_0\mathbf{p}$. The factor $-i$ leads to an additional phase shift of $-90°$ for $\mathbf{J}$. The phase shift for the current then reads $\Delta\varphi(\mathbf{J}, \mathbf{H}_i) = \Delta\varphi(\mathbf{p}, \mathbf{E}_i) - 90°$, with $\Delta\varphi(\mathbf{p}, \mathbf{E}_i)$ obtained directly from the oscillator model (see the blue and orange lines in Fig. 1).

Let us now discuss the average and the instantaneous forces in Eqs. (8) and (9). This will allow us to understand the different force dynamics that one can obtain. Overall, the amplitude of the average and instantaneous terms scales with the SCS of the object as $\mathbf{J} \sim \sqrt{\text{SCS}}$ [61]. Additionally, the
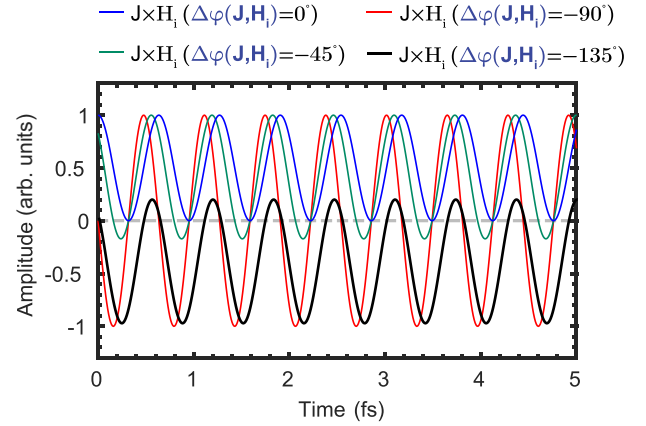

FIG. 2. Electromagnetic forces on an isolated Ag spherical nanoparticle with radius $R = 10$ nm due to the magnetic component of the Lorenz force in Eq. (9) for different phase shifts $\Delta\varphi(\mathbf{J}, \mathbf{H}_i)$. The dynamics for each curve is normalized with respect to the corresponding absolute maximum.

average force is proportional to $\cos[\Delta\varphi(\mathbf{J}, \mathbf{H}_i)]$ [see Eq. (8)]. Consequently, when the frequency of the incident wave ω_0 matches the resonance frequency ω_r of the system, the phase shift $\Delta\varphi(\mathbf{J}, \mathbf{H}_i) = 0°$, and the average force is equal to the amplitude of the oscillating component of the force, which follows from Eqs. (8) and (9). Therefore, the optical force is positive at all instances of time; see Fig. 2, where Eq. (9) is plotted for different $\Delta\varphi(\mathbf{J}, \mathbf{H}_i)$. In this graph, we normalized the force with respect to its maximum to highlight the overall transition between purely positive and alternating positive and negative forces. On the other hand, for a plane wave excitation with a frequency $\omega_0 \ll \omega_r$, the average force will be equal to zero because the phase shift $\Delta\varphi(\mathbf{J}, \mathbf{H}_i) \to -90°$. This case of zero average force with $\omega_0 \ll \omega_r$ is shown as a red line in Fig. 2. Additionally, we indicate the phase shift $\Delta\varphi(\mathbf{J}, \mathbf{H}_i) = -45°$ as a green line, which corresponds to the intermediate case where $\hbar\omega_0 \approx 3.66$ eV. In this situation, the force is overall positive, with short periods of time when the force reaches negative values. However, this work aims to achieve *optical pulling* with a negative *average* force. Equation (8) indicates that this would be the case if $\Delta\varphi(\mathbf{J}, \mathbf{H}_i)$ surpassed $\pm 90°$, which is not possible for monochromatic illumination (Fig. 1). Indeed, if we plot the dynamics of the force for $\Delta\varphi(\mathbf{J}, \mathbf{H}_i) = -135°$, the average force becomes negative (black solid line in Fig. 2).

In the following section we will show how to achieve a phase shift that is inaccessible in Fig. 1 and obtain optical pulling over a series of consecutive optical cycles using a dynamic phase variation based on electromagnetic interference and beating.

III. UNLOCKING PHASE VARIATIONS

As seen from Fig. 1, the phase $\Delta\varphi(\mathbf{J}, \mathbf{H}_i)$ that controls the sign of the force appears to be locked by the structure and the monochromatic illumination. Changing the geometry of the structure does not solve the issue: The phase is still locked within the bounds [67]. If we manage to change the phase such that it surpasses $\pm 90°$, the force can be reverted, which
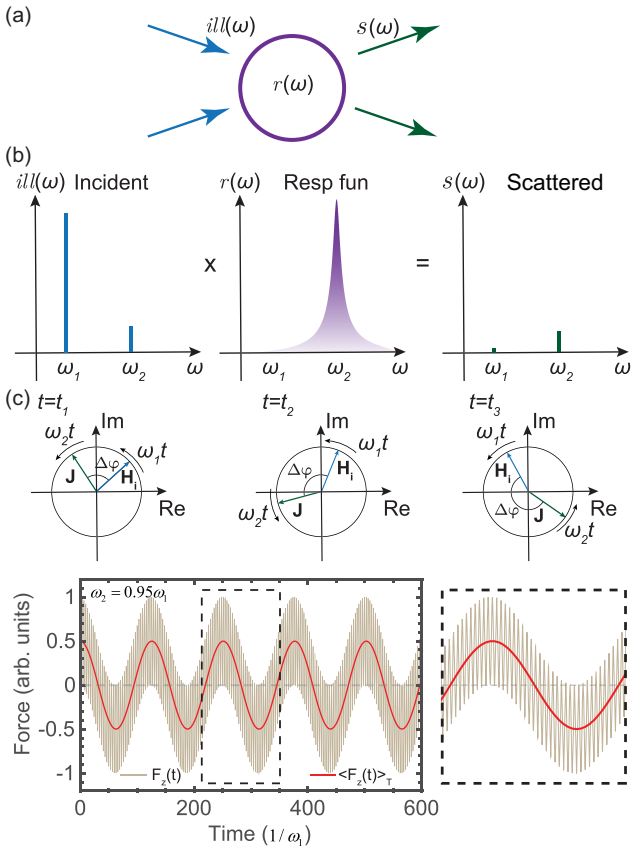
FIG. 3. (a) Schematics of the spectral representation of an object with a response function $r(\omega)$, illuminated with an incident wave having the spectrum ill(ω). The resulting scattering spectrum $s(\omega)$ for a linear system is then $s(\omega) = \text{ill}(\omega)r(\omega)$. (b) Transformation of an incident spectrum into a scattering one by a structure with a high quality factor. (c) The incident magnetic field $\mathbf{H}_\text{i}$ and the excited current $\mathbf{J}$ oscillating at frequencies ω_1 and ω_2 have a dynamically varying phase shift $\Delta\varphi(\mathbf{J}, \mathbf{H}_\text{i})$ and produce an optical force that has a beatinglike dynamics.

follows from Eq. (9). This can be achieved by simultaneously using two frequency components, ω_1 and ω_2, in the illumination spectrum ill(ω) [see Figs. 3(a) and 3(b)]. Let us assume that the structure has a single resonance frequency response function $r(\omega)$ (one can link this response to the polarizability of a small plasmonic object). In this example, the component of the incident field with frequency ω_1 is off resonant and has a large amplitude, while the component ω_2 is at the structure's resonance and is chosen to be much weaker than the first component. Since, for a linear system, the scattered spectrum

$$s(\omega) = \text{ill}(\omega)r(\omega), \qquad (12)$$

the scattered component at frequency ω_1 is expected to be suppressed since it is off resonant, whereas the component ω_2 remains strong, as seen in the right panel of Fig. 3(b). Let us now estimate the dynamics of the optical force in this case. The incident magnetic field in Eq. (9) can be considered to be composed mostly of the component at frequency ω_1, whereas the current $\mathbf{J}$ is dominated by frequency ω_2. Since the current and the incident field now oscillate at different frequencies, the phase shift between them dynamically varies

as $\Delta\varphi(\mathbf{J}, \mathbf{H}_\text{i}) = (\omega_2 - \omega_1)t$. Therefore, we have unlocked the classical limit on the phase, which can now dynamically span the whole $360°$ range.

For a subwavelength structure, it follows from Eq. (8) that the total force will change sign with time since the phase shift has different values at different instants of time [see Fig. 3(c)]. Such a force dynamics has the form of beating at frequency $\omega_2 - \omega_1$, as shown by a gray line in Fig. 3(c). For this example, we considered $\omega_2 = 0.95\omega_1$. We also performed an averaging of the force for this plot (red curve) by separately finding the average within each consecutive oscillation. The dynamics of the magnified area in Fig. 3(c) is shown on the right. As a remarkable result, the optical force is now directed toward the source of the illumination and does not change sign for about 10 optical cycles. In the next section, we exploit this effect with optical pulses instead of a continuous wave illumination.

IV. PHASE VARIATION WITH A PULSE

We now excite the spherical nanoparticle considered in Sec. II with a femtosecond Gaussian pulse with a width of $\tau = 22$ fs. The form of the pulse at the center of the structure (in the paraxial approximation) is

$$\mathbf{E}_\text{i}(t) = \mathbf{A} \exp[-t^2/(2\tau^2)] \cos(\omega_0 t), \qquad (13)$$

where $\mathbf{A}$ is the amplitude of the field. The power transmitted by this pulse given by Eq. (13) can be found as

$$P = c\varepsilon_0 \int_{-\infty}^{+\infty} |\mathbf{E}_\text{i}(t)|^2 dt = c\varepsilon_0 \frac{|\mathbf{A}|^2\tau}{2}\sqrt{\pi}\left[1 + \exp\left(-\omega_0^2\tau^2\right)\right]. \qquad (14)$$

In the following, we will present the optical force dynamics normalized with respect to the pulse power. For the force dynamics $F_z(t)$ divided by the pulse power, the units are N m^2/J (here, J = joule).

With a pulse, we aim to produce an illumination spectrum that is asymmetric with respect to the response function of the object, similar to the example shown in Fig. 3(b). This can be done by detuning the pulse from the resonance, as shown in the inset of Fig. 4(c). In this case, $\hbar\omega_0 = 3.54$ eV, which corresponds to the phase shift $\Delta\varphi(\mathbf{J}, \mathbf{H}_\text{i}) = -82.5°$ (see Fig. 1). For a subwavelength system, the spectrum of the current $\mathbf{J}(\omega)$ can be obtained as $\mathbf{J}(\omega) \sim -i\omega\alpha(\omega)\mathbf{E}_\text{i}(\omega)$, where $\alpha(\omega)$ is the polarizability of the object. This is similar to Eq. (12), where the response function of the structure is multiplied by the spectrum of the incident field. Therefore, the results developed in Sec. III can also be applied here. The resulting current spectrum is shown in green in the inset of Fig. 4(c). Let us now analyze the dynamics of the signal in the time domain. For the incident field, we observe in Fig. 4(a) a Gaussian pulse profile given by Eq. (13). To obtain the dynamics of the current, we perform an inverse Fourier transform of the scattered signal calculated in the frequency domain with the surface integral equation (SIE) method [69] as described in Refs. [36,37]. As can be seen from Fig. 4(a), the current oscillations last longer than the oscillations of the incident field. In addition, the current is retarded with respect to the incident field, which is a classical effect seen in resonant systems [67,70]. By comparing the dynamics of the current
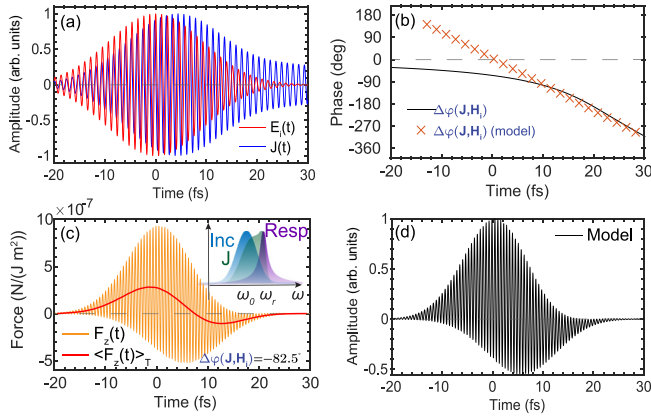
FIG. 4. (a) Dynamics of the incident electric field along with the current excited within the structure. (b) Phase shift between the current and incident magnetic field calculated from (a) and from the model given by Eq. (15) with $v_{\phi,0}$ found by fitting. (c) Dynamics of the force found with the full-wave simulations for the excitation close to the resonance, as shown in the inset. The red curve shows the time average calculated for each consecutive cycle. (d) The profile of the force found by solving the harmonic oscillator equations with a pulsed excitation profile and using only the dipolar approximation in Eq. (9).

and of the incident field in Fig. 4(a), one notices that the phase shift between the two is not the same during the pulse cycle. Indeed, at time instances close to $t = -20$ fs the current and incident field are almost in phase, whereas close to $t = 20$ fs the two are out of phase. This effect can be explained by the dynamic phase variation highlighted previously. Indeed, since the current has a frequency response that is maximized at a slightly higher frequency, closer to ω_r, the phase shift between the current and incident field changes with time. In the first approximation, one can assume that the incident field oscillates at frequency ω_0 and the current oscillates at ω_J, which is the maximum of the curve in Fig. 4(c). In our case, we found $\hbar\omega_J = 3.66$ eV. Then, the velocity of the phase shift can be found analytically as approximately $v_\varphi = \omega_0 - \omega_J$. In Fig. 4(b) we plot the phase shift between the current and the incident magnetic field (magnetic and electric fields oscillate in phase) as a function of time and approximate this dependence with the model

$$\Delta\varphi(\mathbf{J}, \mathbf{H}_i) = v_\varphi t + v_{\varphi,0}. \tag{15}$$

As can be seen in Fig. 4(d), this model describes well the dynamics of the phase shift at time instances above $t > 5$ fs. The dynamic variation of the phase shift leads to nontrivial dynamics for the optical force [see Fig. 4(c)]. This dynamics is obtained with the full-wave calculation of fields on the surface of the structure and involves the calculation of the Maxwell stress tensor in the Abraham form, as discussed in Refs. [71,72]. Additionally, we perform a volumetric integration of the momentum of the electromagnetic fields inside the structure to find the dynamics of the force [34]. As can be seen, the optical force is overall positive from the beginning of the pulse until approximately $t = 8$ fs. After this time, the force switches to negative values. This can be better visualized by looking at the average of the force that we calculated for

each consecutive cycle. By comparing Figs. 4(b) and 4(c), we notice that as the phase shift surpasses $-90°$, the optical force becomes negative, as predicted by Eq. (8).

To further verify the correctness of our simulations, we created a simplified model, in which the incident field dynamics is taken from Eq. (13) and the dynamics of current $\mathbf{J}$ is found by solving the harmonic oscillator model in the time domain by extracting the properties of the oscillator (width, resonance frequency) from Fig. 1. Then, from Eq. (9) we find an approximate dynamics of the force and plot its normalized values in Fig. 4(d). As can be seen, there is almost a perfect correspondence between the forms of the approximate solution and the full-wave results in Fig. 4(c).

V. OFF-RESONANT AND RESONANT EXCITATION WITH A PULSE

Let us now discuss the case when the central frequency of the pulse is much less than the resonant frequency of the structure $\omega_0 \ll \omega_r$ [see Fig. 5(a)]. In this situation, the presence of the resonance will barely affect the response function. Indeed, for the Lorentzian function

$$L(\omega) \sim \frac{1}{\omega_r^2 - \omega^2 - i\gamma\omega} \overset{\omega \ll \omega_r}{\sim} \frac{1}{\omega_r^2}. \tag{16}$$

Therefore, the response function $r(\omega) \sim$ const. Consequently, the spectrum of the incident field and the spectrum of the current $\mathbf{J}$ have peaks at almost the same frequencies [the spectrum of the current is therefore not shown in Fig. 5(a)]. Let us consider the dynamics of the optical force under off-resonant excitation. For the Gaussian pulse considered before with $\hbar\omega_0 = 3.25$ eV, the dynamics of the force calculated with the full-wave simulation is shown in Fig. 5(a). We see that the force oscillates from positive to negative values during the entire pulse duration. Such dynamics can be explained if we assume that the incident field and current oscillate at the same single frequency. Then, the situation is the same as that in
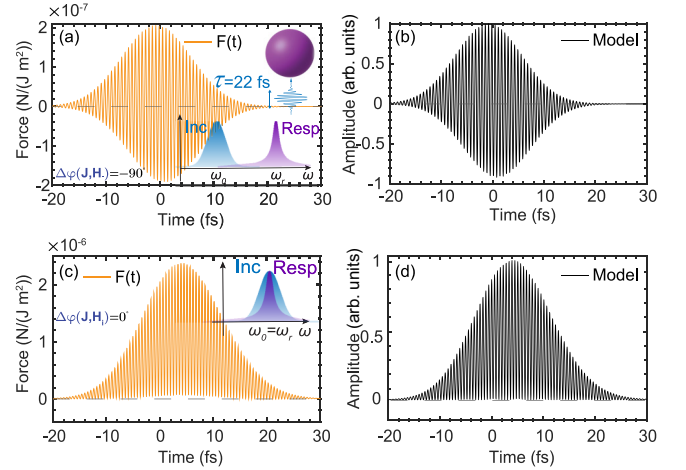

FIG. 5. (a) Dynamics of the optical force given by full-wave simulations for off-resonant excitation. (b) Dynamics of the force for off-resonant excitation obtained from the dipolar approximation in Eq. (9). (c) Dynamics of the optical force given by full-wave simulations for resonant excitation. (d) Dynamics of the force for resonant excitation obtained from the dipolar approximation in Eq. (9).

Fig. 2 for $\Delta\varphi(\mathbf{J}, \mathbf{H}_i) = -90°$, where we observed the same positive to negative oscillations. To ensure the correctness of our simulations, we also test in Fig. 5(b) the profile of the force with the model based on Eq. (9), as discussed in the previous section. As can be seen, the profile of the force given by the model matches that obtained with the full-wave simulations.

For the resonant excitation, where $\omega_0 = \omega_r$, the current and the incident field also oscillate at the same frequency [see Fig. 5(c)]. Here, we do not show the spectrum of the current, as it only slightly deviates from that of the incident field. The dynamics of the force obtained with the full-wave analysis is shown in Fig. 5(c). As can be seen, the force is positive during the entire pulse duration. This effect can be explained if we assume that the current and the field oscillate at the same frequency and $\Delta\varphi(\mathbf{J}, \mathbf{H}_i) = 0°$ (because of the resonant excitation). Then, the dynamics resembles that shown in Fig. 2 for $\Delta\varphi(\mathbf{J}, \mathbf{H}_i) = 0°$. To verify the correctness of our simulations, we again show the profile of the force in Fig. 5(d) with a dipolar model and find very good agreement between Figs. 5(c) and 5(d).

VI. CONCLUSIONS AND OUTLOOK

By utilizing pulsed excitations, we were able to create conditions such that the maximum of the excited current and the maximum of the incident field did not match spectrally. Therefore, the phase shift between these two quantities became time dependent, with the ability to span the whole 2π range. In this way, we overcame the classical limitation on this phase shift and temporally reversed the optical force.

A limitation of the obtained pulling force, however, is related to its very short duration of only about 10 fs in this case. A possible way to increase this duration would be to decrease the driving frequency. Indeed, due to the scalability of Maxwell's equations, one can decrease the operational frequency while increasing the size of the object. In this case, the effect of the negative force will last longer. However, more power will be required to act on larger objects.

We found possible applications of the observed dynamic phase variation in other types of photonic systems. For instance, the proposed mechanism may serve as a promising platform for beam steering applications. Indeed, in optical systems such as metasurfaces, the ability to control the phase shift opens the way for comprehensive 3D scans of the space surrounding the metasurface, as well as dispersion engineering and time-varying optical transformations.

Finally, more exotic manipulations of objects in time can be attained by taking into consideration higher-order multiples. Further inspiration can be taken from existing works on space manipulation [73–75] and rotations [76–79] of nano-objects with multipoles.

[1] J. Kepler, *De cometis libelli tres* (typis Andreae Apergeri, 1619).

[2] O. Gingerich, Kepler's place in astronomy, Vistas Astron. **18**, 261 (1975).

[3] A. Ashkin, Acceleration and trapping of particles by radiation pressure, Phys. Rev. Lett. **24**, 156 (1970).

[4] A. Ashkin, J. M. Dziedzic, J. E. Bjorkholm, and S. Chu, Observation of a single-beam gradient force optical trap for dielectric particles, Opt. Lett. **11**, 288 (1986).

[5] Y. Yang, Y. Ren, M. Chen, Y. Arita, and C. Rosales-Guzmán, Optical trapping with structured light: A review, Adv. Photon. **3**, 034001 (2021).

[6] Y. Zhang, C. Min, X. Dou, X. Wang, H. P. Urbach, M. G. Somekh, and X. Yuan, Plasmonic tweezers: For nanoscale optical trapping and beyond, Light: Sci. Appl. **10**, 59 (2021).

[7] X. Han, V. G. Truong, P. S. Thomas, and S. N. Chormaic, Sequential trapping of single nanoparticles using a gold plasmonic nanohole array, Photon. Res. **6**, 981 (2018).

[8] P. Zemánek, G. Volpe, A. Jonáš, and O. Brzobohatý, Perspective on light-induced transport of particles: From optical forces to phoretic motion, Adv. Opt. Photon. **11**, 577 (2019).

[9] H. Li, Y. Cao, L.-M. Zhou, X. Xu, T. Zhu, Y. Shi, C.-W. Qiu, and W. Ding, Optical pulling forces and their applications, Adv. Opt. Photon. **12**, 288 (2020).

[10] W. Zhang, L. Huang, C. Santschi, and O. J. F. Martin, Trapping and sensing 10 nm metal nanoparticles using plasmonic dipole antennas, Nano Lett. **10**, 1006 (2010).

[11] T. Chantakit, C. Schlickriede, B. Sain, F. Meyer, T. Weiss, N. Chattham, and T. Zentgraf, All-dielectric silicon metalens for two-dimensional particle manipulation in optical tweezers, Photon. Res. **8**, 1435 (2020).

[12] Y. Shi, X. Xu, M. Nieto-Vesperinas, Q. Song, A. Q. Liu, G. Cipparrone, Z. Su, B. Yao, Z. Wang, C.-W. Qiu, and X. Cheng, Advances in light transverse momenta and optical lateral forces, Adv. Opt. Photon. **15**, 835 (2023).

[13] L. Zhu, Y. Tai, H. Li, H. Hu, X. Li, Y. Cai, and Y. Shen, Multidimensional optical tweezers synthesized by rigid-body emulated structured light, Photon. Res. **11**, 1524 (2023).

[14] S.-H. Lee, Y. Roichman, and D. G. Grier, Optical solenoid beams, Opt. Express **18**, 6988 (2010).

[15] A. Novitsky, C.-W. Qiu, and H. Wang, Single gradientless light beam drags particles as tractor beams, Phys. Rev. Lett. **107**, 203601 (2011).

[16] O. Brzobohatý, V. Karásek, M. Šiler, L. Chvátal, T. Čižmár, and P. Zemánek, Experimental demonstration of optical transport, sorting and self-arrangement using a 'tractor beam,' Nat. Photon. **7**, 123 (2013).

[17] V. Shvedov, A. R. Davoyan, C. Hnatovsky, N. Engheta, and W. Krolikowski, A long-range polarization-controlled optical tractor beam, Nat. Photon. **8**, 846 (2014).

[18] M. Sonnleitner, M. Ritsch-Marte, and H. Ritsch, Attractive optical forces from blackbody radiation, Phys. Rev. Lett. **111**, 023601 (2013).

[19] M. Levin, A. P. McCauley, A. W. Rodriguez, M. T. Homer Reid, and S. G. Johnson, Casimir repulsion between metallic objects in vacuum, Phys. Rev. Lett. **105**, 090403 (2010).

[20] D. E. Fernandes and M. G. Silveirinha, Optical tractor beam with chiral light, Phys. Rev. A **91**, 061801(R) (2015).

[21] D. E. Fernandes and M. G. Silveirinha, Single-beam optical conveyor belt for chiral particles, Phys. Rev. Appl. **6**, 014016 (2016).

[22] K. Ding, J. Ng, L. Zhou, and C. T. Chan, Realization of optical pulling forces using chirality, Phys. Rev. A **89**, 063825 (2014).

[23] A. Mizrahi and Y. Fainman, Negative radiation pressure on gain medium structures, Opt. Lett. **35**, 3405 (2010).

[24] M. I. Petrov, S. V. Sukhov, A. A. Bogdanov, A. S. Shalin, and A. Dogariu, Surface plasmon polariton assisted optical pulling force, Laser Photon. Rev. **10**, 116 (2016).

[25] N. Kostina, M. Petrov, V. Bobrovs, and A. S. Shalin, Optical pulling and pushing forces via Bloch surface waves, Opt. Lett. **47**, 4592 (2022).

[26] Y.-J. L. Chu, E. M. Jansson, and G. A. Swartzlander, Measurements of radiation pressure owing to the grating momentum, Phys. Rev. Lett. **121**, 063903 (2018).

[27] C. Pfeiffer and A. Grbic, Generating stable tractor beams with dielectric metasurfaces, Phys. Rev. B **91**, 115408 (2015).

[28] A. S. Shalin, S. V. Sukhov, A. A. Bogdanov, P. A. Belov, and P. Ginzburg, Optical pulling forces in hyperbolic metamaterials, Phys. Rev. A **91**, 063830 (2015).

[29] N. Wang, R.-Y. Zhang, Q. Guo, S. Wang, G. P. Wang, and C. T. Chan, Optical pulling using topologically protected one way transport surface-arc waves, Phys. Rev. B **105**, 014104 (2022).

[30] A. A. Bogdanov, A. S. Shalin, and P. Ginzburg, Optical forces in nanorod metamaterial, Sci. Rep. **5**, 15846 (2015).

[31] W. D. Phillips, Nobel lecture: Laser cooling and trapping of neutral atoms, Rev. Mod. Phys. **70**, 721 (1998).

[32] S. Chu, Nobel lecture: The manipulation of neutral particles, Rev. Mod. Phys. **70**, 685 (1998).

[33] C. N. Cohen-Tannoudji, Nobel lecture: Manipulating atoms with photons, Rev. Mod. Phys. **70**, 707 (1998).

[34] A. Kiselev, K. Achouri, and O. J. F. Martin, Electromagnetic forces in the time domain, Opt. Express **30**, 32215 (2022).

[35] J. Butet, P.-F. Brevet, and O. J. F. Martin, Optical second harmonic generation in plasmonic nanostructures: From fundamental principles to advanced applications, ACS Nano **9**, 10545 (2015).

[36] G. D. Bernasconi, J. Butet, and O. J. F. Martin, Dynamics of second-harmonic generation in a plasmonic silver nanorod, ACS Photon. **5**, 3246 (2018).

[37] A. Kiselev, G. D. Bernasconi, and O. J. F. Martin, Modes interplay and dynamics in the second harmonic generation of plasmonic nanostructures, Opt. Express **27**, 38708 (2019).

[38] M. Partanen, H. Lee, and K. Oh, Radiation pressure measurement using a macroscopic oscillator in an ambient environment, Sci. Rep. **10**, 20419 (2020).

[39] M. Partanen, H. Lee, and K. Oh, Quantitative in situ measurement of optical force along a strand of cleaved silica optical fiber induced by the light guided therewithin, Photon. Res. **9**, 2016 (2021).

[40] M. Mansuripur, Radiation pressure and the linear momentum of light in dispersive dielectric media, Opt. Express **13**, 2245 (2005).

[41] V. B. Braginsky, S. E. Strigin, and S. P. Vyatchanin, Analysis of parametric oscillatory instability in power recycled LIGO interferometer, Phys. Lett. A **305**, 111 (2002).

[42] H. Rokhsari, T. J. Kippenberg, T. Carmon, and K. J. Vahala, Radiation-pressure-driven micro-mechanical oscillator, Opt. Express **13**, 5293 (2005).

[43] T. J. Kippenberg, H. Rokhsari, T. Carmon, A. Scherer, and K. J. Vahala, Analysis of radiation-pressure induced mechanical oscillation of an optical microcavity, Phys. Rev. Lett. **95**, 033901 (2005).

[44] G. Anetsberger, O. Arcizet, Q. P. Unterreithmeier, R. Rivière, A. Schliesser, E. M. Weig, J. P. Kotthaus, and T. J. Kippenberg, Near-field cavity optomechanics with nanomechanical oscillators, Nat. Phys. **5**, 909 (2009).

[45] A. Schliesser, P. Del'Haye, N. Nooshi, K. J. Vahala, and T. J. Kippenberg, Radiation pressure cooling of a micromechanical oscillator using dynamical backaction, Phys. Rev. Lett. **97**, 243905 (2006).

[46] T. J. Kippenberg and K. J. Vahala, Cavity opto-mechanics, Opt. Express **15**, 17172 (2007).

[47] T. J. Kippenberg and K. J. Vahala, Cavity optomechanics: Backaction at the mesoscale, Science **321**, 1172 (2008).

[48] H. Lü, Y. Jiang, Y.-Z. Wang, and H. Jing, Optomechanically induced transparency in a spinning resonator, Photon. Res. **5**, 367 (2017).

[49] J. Söding, R. Grimm, Y. B. Ovchinnikov, P. Bouyer, and C. Salomon, Short-distance atomic beam deceleration with a stimulated light force, Phys. Rev. Lett. **78**, 1420 (1997).

[50] M. T. Cashen and H. Metcalf, Bichromatic force on helium, Phys. Rev. A **63**, 025406 (2001).

[51] L. Yatsenko and H. Metcalf, Dressed-atom description of the bichromatic force, Phys. Rev. A **70**, 063402 (2004).

[52] F. Peano, J. Vieira, L. O. Silva, R. Mulas, and G. Coppa, All-optical trapping and acceleration of heavy particles, New J. Phys. **10**, 033028 (2008).

[53] M. M. Rahman, A. A. Sayem, M. R. C. Mahdy, M. E. Haque, R. Islam, S. T.-u.-R. Chowdhury, and M. A. Matin, Tractor beam for fully immersed multiple objects: Long distance pulling, trapping, and rotation with a single optical set-up, Ann. Phys. (Berlin, Ger.) **527**, 777 (2015).

[54] S. E. Galica, L. Aldridge, and E. E. Eyler, Four-color stimulated optical forces for atomic and molecular slowing, Phys. Rev. A **88**, 043418 (2013).

[55] H. Metcalf, Colloquium: Strong optical forces on atoms in multifrequency light, Rev. Mod. Phys. **89**, 041001 (2017).

[56] A. A. Ambardekar and Y. Li, Optical levitation and manipulation of stuck particles with pulsed optical tweezers, Opt. Lett. **30**, 1797 (2005).

[57] J.-L. Deng, Q. Wei, Y.-Z. Wang, and Y.-Q. Li, Numerical modeling of optical levitation and trapping of the "stuck" particles with a pulsed optical tweezers, Opt. Express **13**, 3673 (2005).

[58] B. J. Roxworthy and K. C. Toussaint, Femtosecond-pulsed plasmonic nanotweezers, Sci. Rep. **2**, 660 (2012).

[59] J. J.-K. Chen, W.-Y. Chiang, T. Kudo, A. Usman, and H. Masuhara, Nanoparticle assembling dynamics induced by pulsed optical force, Chem. Rec. **21**, 1473 (2021).

[60] J. C. Shane, M. Mazilu, W. M. Lee, and K. Dholakia, Effect of pulse temporal shape on optical trapping and impulse transfer using ultrashort pulsed lasers, Opt. Express **18**, 7554 (2010).

[61] J. D. Jackson, *Classical Electrodynamics* (Wiley, New York, 1999).

[62] S. Lepeshov and A. Krasnok, Virtual optical pulling force, Optica **7**, 1024 (2020).

[63] J. Chen, J. Ng, Z. Lin, and C. T. Chan, Optical pulling force, Nat. Photon. **5**, 531 (2011).

[64] A. Lovera, B. Gallinet, P. Nordlander, and O. J. Martin, Mechanisms of Fano resonances in coupled plasmonic systems, ACS Nano **7**, 4527 (2013).

[65] C. F. Bohren and D. R. Huffman, *Absorption and Scattering of Light by Small Particles* (Wiley, Hoboken, NJ, 2008).

[66] B. Abasahl, C. Santschi, and O. J. F. Martin, Quantitative extraction of equivalent lumped circuit elements for complex plasmonic nanostructures, ACS Photon. **1**, 403 (2014).

[67] T. V. Raziman and O. J. F. Martin, Does the real part contain all the physical information? J. Opt. **18**, 095002 (2016).

[68] S. A. Maier, *Plasmonics: Fundamentals and Applications* (Springer, New York, NY, 2007), Vol. 1.

[69] A. M. Kern and O. J. F. Martin, Surface integral formulation for 3D simulations of plasmonic and high permittivity nanostructures, J. Opt. Soc. Am. A **26**, 732 (2009).

[70] W. Zhang and O. J. F. Martin, A universal law for plasmon resonance shift in biosensing, ACS Photon. **2**, 144 (2015).

[71] A. Kiselev, K. Achouri, and O. J. F. Martin, Dynamics of optical forces and torques in plasmonic systems: A surface integral equation, Proc. SPIE **11463**, 1146313 (2020).

[72] A. Ji, T. V. Raziman, J. Butet, R. P. Sharma, and O. J. F. Martin, Optical forces and torques on realistic plasmonic nanostructures: A surface integral approach, Opt. Lett. **39**, 4699 (2014).

[73] A. Kiselev, K. Achouri, and O. J. F. Martin, Multipole interplay controls optical forces and ultra-directional scattering, Opt. Express **28**, 27547 (2020).

[74] K. Achouri, A. Kiselev, and O. J. F. Martin, Multipolar origin of electromagnetic transverse force resulting from two-wave interference, Phys. Rev. B **102**, 085107 (2020).

[75] M. Riccardi, A. Kiselev, K. Achouri, and O. J. F. Martin, Multipolar expansions for scattering and optical force calculations beyond the long wavelength approximation, Phys. Rev. B **106**, 115428 (2022).

[76] Y. Zhou, X. Xu, Y. Zhang, M. Li, S. Yan, M. Nieto-Vesperinas, B. Li, C.-W. Qiu, and B. Yao, Observation of high-order imaginary Poynting momentum optomechanics in structured light, Proc. Natl. Acad. Sci. USA **119**, e2209721119 (2022).

[77] Y. Zhou, Y. Zhang, X. Xu, M. Nieto-Vesperinas, S. Yan, M. Li, W. Gao, Y. Zhang, and B. Yao, Optical forces on multipoles induced by the Belinfante spin momentum, Laser Photon. Rev. **17**, 2300245 (2023).

[78] X. Xu, M. Nieto-Vesperinas, Y. Zhou, Y. Zhang, M. Li, F. J. Rodríguez-Fortuño, S. Yan, and B. Yao, Gradient and curl optical torques, Nat. Commun. **15**, 6230 (2024).

[79] K. Achouri, M. Chung, A. Kiselev, and O. J. Martin, Multipolar pseudochirality-induced optical torque, ACS Photon. **10**, 3275 (2023).